Cross-relaxation and phonon bottleneck effects on magnetization dynamics in LiYF$_4$:Ho^{3+}

S. Bertaina,[1,2] B. Barbara,[1] R. Giraud,[1,3] B. Z. Malkin,[4] M. V. Vanuynin,[4] A. I. Pominov,[4] A. L. Stolov,[4] and A. M. Tkachuk[5]

[1]*Laboratoire de Magnétisme Louis Néel, CNRS, BP 166, 38042 Grenoble CEDEX-09, France*

[2]*Ecole Nationale Supérieure de Physique de Grenoble, 38402, St-Martin d'Hères, France*

[3]*LPN, CNRS, 91460-Marcoussis, France*

[4]*Kazan State University, Kazan 420008, Russian Federation*

[5]*S.I. Vavilov State Optical Institute, St. Petersburg 199034, Russian Federation*

(Received 5 July 2006; revised manuscript received 2 October 2006; published 17 November 2006)

Frequency and dc magnetic field dependences of dynamic susceptibility in diluted paramagnets LiYF$_4$:Ho^{3+} have been measured at liquid helium temperatures in ac and dc magnetic fields parallel to the symmetry axis of a tetragonal crystal lattice. Experimental data are analyzed in the framework of the microscopic theory of relaxation rates in the manifold of 24 electron-nuclear sublevels of the lowest non-Kramers doublet and the first excited singlet in the Ho^{3+} ground multiplet $^5I_8$ split by the crystal field of S_4 symmetry. The one-phonon transition probabilities were computed using electron-phonon coupling constants calculated in the framework of the exchange charge model and were checked by optical piezospectroscopic measurements. The specific features observed in field dependences of the in- and out-of-phase susceptibilities (humps and dips, respectively) at the crossings (anticrossings) of the electron-nuclear sublevels are well reproduced by simulations when the phonon bottleneck effect and the cross-spin relaxation are taken into account.

I. INTRODUCTION

In 1968 Hellwege *et al.*[1] found an unusual nonmonotonous behavior of the in-phase magnetic susceptibility in parallel dc and ac magnetic fields with narrow maxima at the dc field values corresponding to the crossings of electron-nuclear sublevels of the ground state of diluted Ho^{3+} ions in LaCl$_3$ at the temperature ~ 1 K and frequencies of the ac field in the range 10^2–5×10^3 Hz. Recently, similar data were independently obtained on the dynamic susceptibility of the diluted paramagnet LiYF$_4$:Ho^{3+} (0.1%) in the region of energy level crossings in Ref. 2. This latter study of the anisotropic rare-earth spin dynamics in the classical regime was an extension of subkelvin magnetization measurements, previously used to reveal the role of quantum fluctuations of atomic magnets in the diluted LiYF$_4$:Ho^{3+} system,[3] similarly to the phenomenon of resonant tunneling of single-molecule magnets in presence of a large uniaxial anisotropy.[4] In both Refs. 1 and 2 the observed peculiarities of the susceptibility dynamics, measured at relatively high temperature, relate to predictions of N. Bloembergen and co-workers in their classical study of the cross-relaxation in spin systems[5] stated "…the susceptibility is usually plotted at constant frequency versus applied dc field. There may easily occur a maximum in this plot, because for certain values of the external field some pairs of levels… may become nearly equidistant." The purpose of the present paper is to investigate the microscopic origin of the susceptibility in diluted LiYF$_4$:Ho^{3+} at liquid helium temperatures, taking into account the different effects of crystal field, electron-phonon, and hyperfine interactions, as well as cross-relaxation processes. The extension of this many-body classical dynamics to the low-temperature quantum case was previously adressed in Refs. 2 and 3. Nevertheless, many-spin quantum fluctuations in highly anisotropic systems, such as cotunneling processes, have not been discussed on microscopic grounds up to now. Therefore, to

go further in the analysis of dynamical magnetic hysteresis loops measured at subkelvin temperatures in the strongly out-of-equilibrium quantum regime,[3,6] a clear understanding of the classical spin dynamics in LiYF$_4$:Ho^{3+} is required. The quasiresonant absorption of radio-frequency (5–10 MHz) ultrasound and ac magnetic field energy at the crossing points in the CaWO$_4$:Ho^{3+} crystal was observed in Ref. 7, and some specific peculiarities of ^{19}F nuclear relaxation rates at the crossing points in LiYF$_4$:Ho^{3+} were found in Ref. 8. All these experimental findings give evidence for essential variations of the relaxation rates in the electron-nuclear subsystem by orders of magnitude within the vicinity of energy-level crossing points. In the present work, measurements of frequency, temperature, and dc magnetic field dependences of the dynamic susceptibility in LiYF$_4$ single crystals containing different concentrations of Ho^{3+} ions have been carried out. The experimental data are analyzed in the framework of the microscopic theory of the electron-phonon interaction in a gapped titled system. The existing data on spectral properties of Ho^{3+} ions in LiYF$_4$ (Ref. 9) and additional piezospectroscopic studies described below allowed us to obtain reliable values of electron-phonon coupling constants and rigorous estimates of relaxation rates in the manifold of lower electron-nuclear sublevels of the ground multiplet. Simulations based on the calculated values of kinetic parameters revealed remarkable differences between the computed and measured dependences of the dynamic susceptibility on the external parameters (frequency, temperature, strength of the constant magnetic field). We found it necessary to derive a more thorough theoretical approach accounting for the phonon bottleneck effect and the cross relaxation. A self-consistent description of all specific features of the measured susceptibilities has been achieved using parameters of the phonon and magnetic subsystems which have physical meaning. The paper is arranged as follows: in the next section we derive a general expression of

the dynamic susceptibility; then, we describe in Sec. III the known spectral properties of impurity Ho^{3+} ions in $LiYF_4$ and calculate in Sec. IV electron-phonon coupling constants which are used to compute the relaxation matrix in the space of lower 24 electron-nuclear sublevels of the ground multiplet in the external magnetic field. Section V contains results of experimental studies, and in the last section we compare measured and simulated in- and out-of-phase susceptibilities.

II. THEORY OF THE DYNAMIC MAGNETIC SUSCEPTIBILITY OF A DILUTED PARAMAGNET

The dynamic susceptibility $\chi(\omega)$ of a single paramagnetic ion coupled to a phonon bath in the external magnetic field $\mathbf{B} = \mathbf{B}_0 + \mathbf{B}_1(\omega, t)$, $[\mathbf{B}_1(\omega, t) = \mathbf{B}_1^0 \exp(-i\omega t)]$ is determined by the following expression:

$$\chi_{\alpha\beta}(\omega) = \frac{\text{Tr}[\rho(t)\Delta m_\alpha]}{B_{1\beta}}. \tag{1}$$

Here $\Delta\mathbf{m} = \mathbf{m} - \langle\mathbf{m}\rangle_0$, $\mathbf{m}$ is the operator of the ion magnetic moment, and $\langle\cdots\rangle_0$ defines an average value, corresponding to the equilibrium single-ion density matrix $\rho_0(H_0) = e^{-H_0/kT}/\text{Tr}(e^{-H_0/kT})$ in the absence of a time-dependent field. The time evolution of the density matrix $\rho(t)$ defined in the space of eigenfunctions $|k\rangle$ corresponding to eigenvalues E_k of the Hamiltonian H_0 of the unperturbed electronic (or electron-nuclear) system can be described by the master equation for diagonal elements, $\rho_{nn} = \rho_n$, and by simple exponential decay of nondiagonal matrix elements (the validity of this "secular" approximation was discussed, in particular, in Refs. 10 and 11):

$$\frac{\partial\rho_n}{\partial t} = \sum_k W_{nk}\rho_k, \tag{2}$$

$$\frac{\partial\rho_{nk}}{\partial t} = -(\gamma_{nk} + i\omega_{nk})\rho_{nk} + \frac{i}{\hbar}[\mathbf{m}\mathbf{B}_1(\omega, t), \rho]_{nk},$$

$$[n \neq k, \omega_{nk} = (E_n - E_k)/\hbar]. \tag{3}$$

When working with Eqs. (2) and (3) we implicitly suppose that the equilibrium state is established in the bath much faster than in the electronic subsystem. Besides, we have omitted on the right-hand side of Eq. (2) the terms $-2\,\text{Im}\,\Sigma_{k\neq n}\mathbf{m}\mathbf{B}_1(\omega, t)\rho_{kn}/\hbar$, which do not contribute to the linear response on the weak alternating field $\mathbf{B}_1(\omega, t)$. The off-diagonal elements of the relaxation matrix $W_{nk} = W_{k\to n}$ are the transition probabilities induced by the electron-phonon interaction. For the one-phonon transitions, $W_{m\to k} = w_{mk}[n(\omega_{mk}) + 1]$ if the frequency of the transition $\omega_{mk} > 0$ and $W_{m\to k} = w_{mk}n(\omega_{km})$ if $\omega_{mk} < 0$ where w_{mk} is the probability of the spontaneous transition and $n(\omega_{mk})$ is the phonon occupation number. The diagonal element $W_{nn} = -\Sigma_k W_{kn}$ determines the lifetime of the corresponding state n, and the coherence decay rate equals

$$\gamma_{nk} = -\frac{1}{2}(W_{nn} + W_{kk}) + \Gamma_{nk}, \tag{4}$$

where the first term is caused by finite lifetimes and Γ_{nk} determines all additional contributions to the homogeneous broadening of the $n \to k$ transition.

Considering the energy of interaction with the time-dependent field $-\mathbf{m}\mathbf{B}_1(\omega, t)$ as a perturbation, we solve equations of motion in the linear approximation:

$$\rho_n(t) = \rho_{0n} + \Delta\rho_n(\omega)\mathbf{B}_1 \exp(-i\omega t), \tag{5}$$

where $\Delta\boldsymbol{\rho}_n(0) = \rho_{0n}(\mathbf{m}_{nn} - \langle\mathbf{m}\rangle_0)/kT$

Postulating that the interaction with the phonon bath tends to establish an equilibrium state at the instant value of the magnetic field, $\Sigma_k W_{nk}\rho_{0k}(H_0 - \mathbf{m}\mathbf{B}_1) = 0$, we obtain from Eqs. (2)–(4)

$$\Delta\rho_{\beta,n}(\omega) = \sum_{kp} (i\omega 1 + \mathbf{W})^{-1}_{nk} W_{kp}\Delta m_{\beta,pp}\rho_{0p}/kT, \tag{6}$$

$$\Delta\rho_{\beta,nk}(\omega) = \frac{m_{\beta,nk}(\rho_{0k} - \rho_{0n})}{\hbar(\omega_{nk} - \omega - i\gamma_{nk})}. \tag{7}$$

The dynamic susceptibility (1) takes the form

$$\chi_{\alpha\beta}(\omega) = \chi^0_{\alpha\beta} - \left\{ i\omega\sum_{nk} \Delta m_{\alpha,nn}(i\omega 1 + \mathbf{W})^{-1}_{nk} \times \Delta m_{\beta,kk}\rho_{0k}/kT \right\}$$

$$+ \sum_{n,k\neq n} m_{\alpha,nk}m_{\beta,kn}(\rho_{0k} - \rho_{0n})$$

$$\times \left(\frac{1}{\hbar(\omega_{nk} - \omega - i\gamma_{nk})} - \frac{1}{\hbar\omega_{nk}} \right), \tag{8}$$

where the well-known expression for the static susceptibility,

$$\chi^0_{\alpha\beta} = \sum_n \Delta m_{\alpha,nn}\Delta m_{\beta,nn}\rho_{0n}/kT + \sum_{n,k\neq n} \frac{m_{\alpha,nk}m_{\beta,kn}}{\hbar\omega_{nk}}(\rho_{0k} - \rho_{0n}), \tag{9}$$

has been used. The first line in Eq. (8) coincides with the expression presented in Ref. 12.

In the case of a finite concentration of paramagnetic ions, we have to take into account interactions between the ions (dipole-dipole, dimer, or trimer exchange, virtual phonon exchange) and the finite rate of a heat flow from the phonon reservoir to the helium bath (the phonon bottleneck effect). These interactions between paramagnetic ions induce energy exchange (cross relaxation), and the master equation (2) contains additional nonlinear terms:[5]

$$\dot{\rho}_n = \sum_m W_{nm}\rho_m + \sum_{mpl} [(W^{CR}_{np,lm}\rho_p\rho_m - W^{CR}_{pn,ml}\rho_l\rho_n)$$

$$- (W^{CR}_{np,lm}\rho_p\rho_m - W^{CR}_{pn,ml}\rho_l\rho_n)_{ad}]. \tag{10}$$

Here $W^{CR}_{np,lm}$ is the probability of the simultaneous transitions $m \to l$ of one ion and $p \to n$ of another ion. According to Fermi's golden rule, this transition probability can be written as follows:[5,13]

$$W_{np,lm}^{CR} = \frac{2\pi}{\hbar^2} \langle |\langle n,l|H_{12}|p,m\rangle|^2 \rangle_{Av} \delta(\omega_{pn} - \omega_{lm}), \quad (11)$$

where H_{12} is the Hamiltonian of interaction between the ions and $\langle \cdots \rangle_{Av}$ means a configuration averaging over the distribution of the paramagnetic ions in the crystal lattice. In the particular case of dipole-dipole interactions between rare-earth magnetic moments $\mathbf{m} = g_J \mu_B \mathbf{J}$, μ_B is the Bohr magneton, $\mathbf{J}$ is the total angular momentum, g_J is the Lande factor, and the Hamiltonian H_{12} has the form

$$H_{12} = \frac{(g_J \mu_B)^2}{R^3} [\mathbf{J}_1 \mathbf{J}_2 - 3(\mathbf{J}_1 \mathbf{R})(\mathbf{J}_2 \mathbf{R})/R^2], \quad (12)$$

where $\mathbf{R}$ is the vector connecting the ions. The last term on the right-hand side of Eq. (10), $\langle \cdots \rangle_{ad}$, provides an asymptotical approach to the equilibrium distribution of populations in the electronic system isolated from the phonon bath (in adiabatic conditions) due to the cross-relaxation processes.[5]

Taking into account the distribution of the single-ion energies, we can write the transition probability (11) in the following form:

$$W_{np,lm}^{CR} = \delta^2 \sum_{\alpha\beta\gamma\delta} g_{\alpha\beta\gamma\delta}^{CR}(\omega_{pn} - \omega_{lm}) k_{\alpha\beta\gamma\delta}$$
$$\times (\langle n|J_{1\alpha}|p\rangle\langle l|J_{2\beta}|m\rangle\langle p|J_{1\gamma}|n\rangle\langle m|J_{2\alpha}|l\rangle + \text{c.c.}),$$
$$(13)$$

where $g_{\alpha\beta\gamma\delta}^{CR}(\omega)$ is the cross-relaxation line shape function, δ is the average energy of the interaction in frequency units [we can consider $\delta = (g_J\mu_B)^2/\hbar R_0^3$ with R_0 equal to a lattice constant as a scaling factor], and $k_{\alpha\beta\gamma\delta}$ are the average values of the corresponding dimensionless lattice factors. The Hamiltonian (12) contains only symmetrical products of the components of the angular moments, $J_{1\alpha}J_{2\beta}$, and in a general case there are 21 independent parameters $k_{\alpha\beta\gamma\delta}$. However, this number can be essentially diminished due to symmetry properties of a concrete lattice (similarly to the elastic compliance tensor). In particular, in a case of S_4 local symmetry of paramagnetic ions, we obtain

$$W_{np,lm}^{CR}\delta^{-2} = g_{33}^{CR}k_{33}|J_{1z}^{np}J_{2z}^{lm}|^2 + g_{11}^{CR}k_{11}(|J_{1+}^{np}J_{2-}^{lm} + J_{1-}^{np}J_{2+}^{lm}|^2) + g_{66}^{CR}k_{66}(|J_{1+}^{np}J_{2+}^{lm} - J_{1-}^{np}J_{2-}^{lm}|^2) + g_{12}^{CR}k_{12}(|J_{1+}^{np}J_{2+}^{lm} + J_{1-}^{np}J_{2-}^{lm}|^2) + g_{44}^{CR}k_{44}[|(J_{1+}^{np}$$
$$+ J_{1-}^{np})J_{2z}^{lm} + J_{1z}^{np}(J_{2+}^{lm} + J_{2-}^{lm})|^2 + |(J_{1+}^{np} - J_{1-}^{np})J_{2z}^{lm} + J_{1z}^{np}(J_{2+}^{lm} - J_{2-}^{lm})|^2] + g_{13}^{CR}k_{13}[J_{1z}^{np}J_{2z}^{lm}(J_{1+}^{pn}J_{2-}^{ml} + J_{1-}^{pn}J_{2+}^{ml}) + \text{c.c.}]$$
$$+ g_{16}^{CR}k_{16}[(J_{1+}^{np}J_{2+}^{lm} - J_{1-}^{np}J_{2-}^{lm})(J_{1+}^{pn}J_{2+}^{ml} + J_{1-}^{pn}J_{2-}^{ml}) + \text{c.c.}],$$
$$(14)$$

with $J^{ab} = \langle a|J|b\rangle$. Because a similar expression may be obtained in a case of long-range interactions between the paramagnetic ions through the field of elastic lattice deformations [$H_{12}^d = \Sigma_{pknm} A_{pk}^{nm} C_k^p(1)C_m^n(2)$ where $C_p^k(i)$ is the spherical tensor operating in the space of states of the ion i and A_{pk}^{nm} are the coupling constants[14]] we consider seven factors k_{ab} introduced in Eq. (14) as the phenomenological parameters.

If the system is not far from equilibrium, Eq. (10) can be linearized. We suppose that the adiabatic density matrix is characterized by a single parameter, the adiabatic temperature. The difference

$$T^{-1} - T_{ad}^{-1} = \frac{\sum_n kE_n\Delta\rho_n\mathbf{B}_1 - T^{-1}\langle H_0\Delta\mathbf{mB}_1\rangle_0}{\langle H_0^2\rangle_0 - \langle H_0\rangle_0^2}$$

between the lattice and adiabatic temperatures is determined from the condition that the average values of the electronic energy $H_0 - \mathbf{mB}_1$ obtained with the adiabatic density matrix and with $\rho(t)$ be equal. The master equation in the form (2) and the expression (8) for the dynamic susceptibility remain valid but with the additional contributions to the relaxation matrix

$$W_{nm} = W_{m\to n} + \sum_k W_{nk}^{CR}\left[\delta_{km} - \rho_{0k}\frac{(E_k - \langle H_0\rangle_0)(E_m - \langle H_0\rangle_0)}{\langle H_0^2\rangle_0 - \langle H_0\rangle_0^2}\right],$$
$$(15)$$

where

$$W_{nm}^{CR} = \sum_{lp}(W_{np,lm}^{CR}\rho_{0p} + W_{nm,lp}^{CR}\rho_{0p} - W_{pn,lm}^{CR}\rho_{0n}) \quad (n \neq m).$$
$$(16)$$

Let us now take into account the finite relaxation rate of the phonon subsystem[15] considering equations of motion for the phonon occupation numbers along with Eq. (2):

$$\frac{dn(\omega_{mk})}{dt} = \frac{1}{\tau_{ph}(\omega_{mk})}[n(\omega_{mk}) - n_0(\omega_{mk})]$$
$$+ \frac{w_{mk}N}{P_{mk}\Delta\omega_{mk}}\{\rho_m[n(\omega_{mk}) + 1] - \rho_k n(\omega_{mk})\}.$$
$$(17)$$

Here $n_0(\omega_{mk}) = [\exp(\hbar\omega_{mk}/kT) - 1]^{-1}$ is the equilibrium occupation number of phonons at the resonance frequency $\omega_{mk} > 0$ in the band with width $\Delta\omega_{mk}$, τ_{ph} is the phonon lifetime, N is the number of paramagnetic ions per unit volume, and P_{mk} is the density of states of resonant phonons (for the low-frequency acoustic phonons $P_{mk} = 3\omega_{mk}^2/2\pi^2 v^3$, where v

is the average sound velocity). The stationary solution of the linearized coupled equations (2) and (17) brings about the same results as the solution of Eq. (2) does [see Eq. (8)], but with the renormalized transition probabilities induced by the phonon bottleneck:

$$W_{m \to n}^{(r)} = W_{m \to n} \left[1 + \frac{2\pi^2 v^3 \tau_{ph}(\omega_{mn}) N w_{mn} |\rho_{0m} - \rho_{0n}|}{3\omega_{mn}^2 \Delta\omega_{mn}[1 + i\omega\tau_{ph}(\omega_{mn})]} \right]^{-1}.$$

(18)

To calculate the susceptibility, we need to know, first of all, elements of the relaxation matrix **W**—i.e., the transition probabilities for each pair of states of a paramagnetic ion induced by the electron-phonon interaction. At the next step, the parameters of the cross-relaxation rates and the phonon lifetimes introduced in expressions (14) and (17), respectively, may be determined from a comparison of the calculated real and imaginary parts of the susceptibility (8) with the experimental data.

III. SPECTRAL PROPERTIES OF ISOLATED Ho³⁺ IONS IN LiYF₄

The crystal lattice of $LiYF_4$ has space group C_{4h}^6 with lattice constants $a = 0.5164$ nm and $c = 1.0741$ nm.[16] The Ho^{3+} ions substitute for Y^{3+} ions in the sites with point symmetry S_4, coordinates of the four nearest fluorine ions at the distance $R_1 = 0.2244$ nm relative to the Ho^{3+} ion in the site (000) equal $(x\ y\ z)$, $(-x\ -y\ z)$, $(x\ -y\ -z)$, $(-x\ y\ -z)$, where $x = (t - 1/2)a$, $y = (1/2 - p)a$, $z = -qc$, and $p = 0.2817$; $t = 0.1645$; $q = 0.0813$. The next-nearest fluorine ions are at the distance $R_2 = 0.2297$ nm; they form a deformed tetrahedron as well with $x = ta$, $y = (1/2 - p)a$, and $z = (q - 1/4)c$.

The energy level pattern of the electronic $4f^{10}$ configuration of the Ho^{3+} ion in $LiYF_4$ was studied in quite a few works;[17–19] fragments of this pattern are shown in Fig. 1. The spectrum consists of singlets (Γ_1 and Γ_2) and non-Kramers doublets (Γ_{34}) corresponding to irreducible representations Γ_k of the S_4 group. Being interested in low-temperature magnetic properties of the system, we can consider only the lower part of the energy spectrum described by the parametrized single-ion Hamiltonian operating in the space of 136 products $|LSJJ_z\rangle \otimes |II_z\rangle$ of the electronic and nuclear spin functions (there is only one holmium isotope ^{165}Ho with nuclear spin $I = 7/2$; L, S, and J are the electronic orbital, spin and total angular moments, respectively, and the lowest electronic multiplet is $^5I_8$):

$$H = H_0 + H_{e\text{-}ph}, \quad H_0 = H_{CF} + H_{hf} + H_Z + H_S. \quad (19)$$

Here

$$H_{CF} = a_2 B_2^0 O_2^0 + a_4 (B_4^0 O_4^0 + B_4^4 O_4^4 + B_4^{-4} O_4^{-4})$$
$$+ a_6 (B_6^0 O_6^0 + B_6^4 O_6^4 + B_6^{-4} O_6^{-4}) \quad (20)$$

is the crystal field Hamiltonian [B_p^k are the crystal field parameters, and $O_p^{|k|}$ and $O_p^{-|k|}$ are the real and imaginary Stevens operators, respectively; $a_2 = \alpha = -1/450$, $a_4 = \beta = -1/30030$, $a_6 = \gamma = -5/(189.143^2)$ are the reduced matrix elements of the Stevens operators in the manifold of the pure
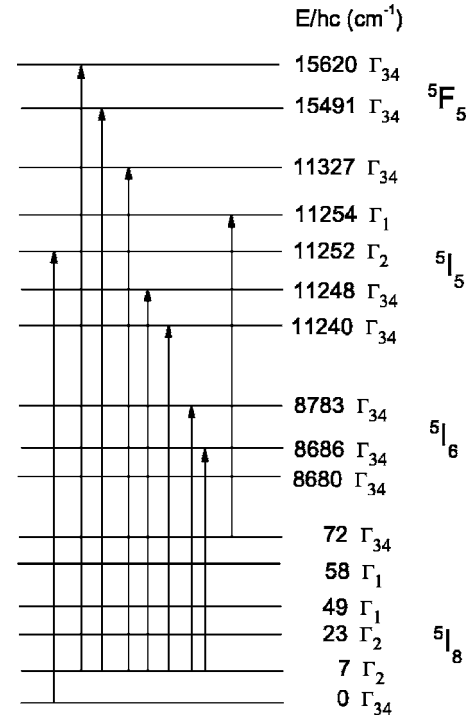

FIG. 1. Optical singlet-doublet transitions in the absorption spectrum of impurity Ho^{3+} ions in $LiYF_4$ explored in the piezospectroscopic measurements.

$^5I_8$ states], H_{hf} is the Hamiltonian of the magnetic hyperfine interaction (the electrostatic quadrupole interaction can be neglected), and $H_Z = g_J\mu_B\mathbf{JB}$ is the electronic Zeeman energy in the magnetic field $\mathbf{B}$; the last two terms in (19), the Hamiltonian of the electron-phonon interaction $H_{e\text{-}ph}$ and the energy of interaction with random lattice strains H_S, are specified below.

As was shown in Ref. 9, the submillimeter electron paramagnetic resonance (EPR) spectra of Ho^{3+} ions in $LiYF_4$ are well described by the effective g factor $g_J = 1.21$ (slightly different from the value 5/4 for the pure $^5I_8$ multiplet), the hyperfine constant $A = 0.795$ GHz, and the crystal field parameters given in Table I.

It should be noted that this set of crystal field parameters is related to the crystallographic system of coordinates (the quantization axis z is parallel to the crystal c axis). This statement is based on the earlier studies of the piezospectroscopic and nonlinear Zeeman effects in $LiYF_4 : Tm^{3+}$ (Refs. 20 and 21), and the anisotropic parastriction in the concentrated paramagnets $LiTmF_4$ (Ref. 22) and $LiErF_4$ (Ref. 23). The calculated hyperfine structure of the ground electronic doublet in an external magnetic field directed along the crystal symmetry axis is shown in Fig. 2. The spectrum consists of the two nearly equidistant groups of electron-nuclear sublevels with positive and negative slopes, respectively. The electron-nuclear sublevels intersect at the magnetic field values $B \cong |m' + m|\Delta B$, where $m, m' = I_z$ and, to first order in A, $\Delta B = A/2g_J\mu_B$. We can distinguish odd (C_{odd}, $|m' - m| = \Delta m = 2k$) and even (C_{even}, $|m' - m| = \Delta m = 2k + 1$) crossing points at magnetic field $B = (2n+1)\Delta B$ and $B = 2n\Delta B$, respectively ($k, n = 0, 1, 2, 3$). The mixing of the ground Γ_{34} doublet with

TABLE I. Crystal field parameters and electron-deformation coupling constants (cm^{-1}).

$p\ k$	B_p^k		$B_p^k(A_g^1)$	$B_p^k(A_g^2)$
	Expt.	Theory		
1	2	3	4	5
2 0	190.4	154	603	−891
4 0	−78.2	−89	125	718
4 4	−657.2	−700	2397	1434
4 −4	−568.6	−613	3700	717
6 0	−3.2	−2.1	113	−416
6 4	−364.0	−322	937	−843
6 −4	−222.3	−265	1738	−889

$p\ k$	$B_p^k(B_g^1)$		$B_p^k(B_g^2)$	
	Expt.	Theory	Expt.	Theory
6	7	8	9	10
2 2	1644	1800	3814	3590
2 −2	1846	2070	−836	−1620
4 2	−454	−780	−1532	−1980
4 −2	1885	3660	1424	1900
6 2	188	230	−243	−730
6 −2	−543	−520	−658	−710
6 6	−858	−740	−1444	−1750
6 −6	−738	−990	−1245	−2010

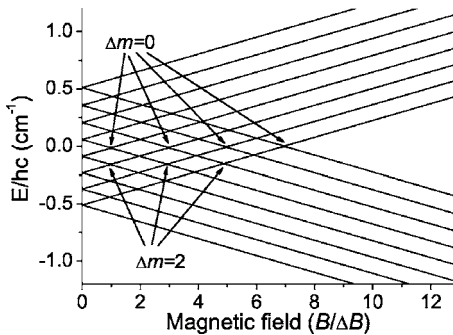| $p\ k$	$B_{pk,1}(E_g)$	$B_{pk,2}(E_g)$	$p\ k$	$B_{pk,1}(E_g)$	$B_{pk,1}(E_g)$
11	12	13	14	15	16
2 1	1951	3595	2 −1	−3595	1951
4 1	−2056	−1996	4 −1	1996	−2056
6 1	−1198	−256	6 −1	256	−1198
4 3	23372	16638	4 −3	16638	−23372
6 3	2093	−1674	6 −3	−1674	−2093
6 5	−7558	−600	6 −5	600	−7558

FIG. 2. Electron-nuclear sublevels of the Ho^{3+} ground doublet $^5I_8(\Gamma_{34})$ in the magnetic field $\mathbf{B} \| c$. The magnetic field strength is given in units of $\Delta B = 23.74$ mT.

the excited singlets Γ_1 and Γ_2 by the magnetic hyperfine interaction opens the gaps at the odd crossing (anticrossing) points with the maximum values for $\Delta m = 2$ of an order of 0.35 GHz (see Fig. 2). However, in addition to the avoided level crossings with $\Delta m = 2$, gaps of comparable values ($\sim$0.28 GHz) were observed at the odd crossing points for the electron-nuclear sublevels with $\Delta m = 0$ in the EPR spectra of the isotopically enriched sample ^{7}LiYF$_4$:Ho^{3+} (0.1%).[9] We suppose that these splittings are induced by random strains due to intrinsic lattice defects. As we shall see below, the presence of random strains is confirmed by some specific features of magnetic field dependences of the dynamic susceptibility as well, and to account for the corresponding random crystal field effects, we introduce the Hamiltonian $H_s = a_2(B_2^2 O_2^2 + B_2^{-2} O_2^{-2})$ with the initial values of the parameters $B_2^2 = \mp 0.4525$ cm^{-1} and $B_2^{-2} = \pm 0.4752$ cm^{-1} which has been already used in Ref. 9 to describe the $\Delta m = 0$ anticrossings

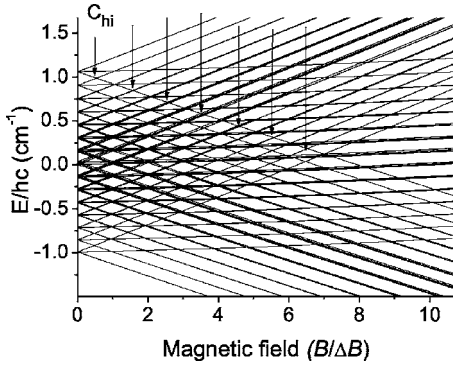FIG. 3. Electron-nuclear sublevels of the ground state of a pair of distant holmium ions in the magnetic field **B**∥*c*. Arrows show half-integer crossings.

observed in the EPR spectra of the sample isotopically enriched in ^{7}Li.

At low temperatures interactions between Ho^{3+} ions play an important role in relaxation processes in the coupled electron-nuclear subsystem.[2,3,6] For a pair of distant Ho^{3+} ions, the energies of the lower 256 electron-nuclear sublevels versus the magnetic field are shown in Fig. 3. This figure presents a plot of the sum of single-ion energies related to a ground Γ_{34} doublet where the random "rhombic" crystal field is taken into account. It is described by the Hamiltonian H_S and mainly affects the electron-nuclear sublevels with the nuclear spin projections $m = \pm 1/2$. The corresponding shifts (about 0.01 cm^{-1}) cause splittings of degenerate energy levels of a dimer which are concentrated close to the centre of gravity of the spectrum in Fig. 3 [in particular, in zero magnetic field, 32 states have zero energy (8 with positive, 8 with negative, and 16 with zero slope in the magnetic field)]. It is well seen in Fig. 3 that there are many additional crossings of the electron-nuclear sublevels in the pair spectrum as compared to the single-ion spectrum (Fig. 2), and the most important qualitative peculiarity is the presence of half-integer crossings (C_{hi}) at the magnetic field values $B \cong (n +1/2)\Delta B$ for $n = 0, 1, \ldots, 6$.

The widths of transitions between the electron-nuclear sublevels of the ground doublet and the first excited singlet measured in EPR spectra are strongly dependent on the holmium concentration[9] at liquid helium temperatures. Assuming a Gaussian distribution, the inhomogeneous broadening can be defined by the full width at half maximum (FWHM) of 175 MHz.[9] According to Ref. 24, the frequencies of the resonance transitions of the two nonequivalent nearest-neighbor fluorine nuclei in the superhyperfine $^5F_5$-$^5I_8$ spectrum equal 29.85 and 36.86 MHz. The corresponding widths of Ho^{3+} energy levels due to the superhyperfine interactions may be estimated as 130 MHz, and the total linewidths at low concentrations ($\sim 0.1\%$) are close to 300 MHz. The magnetic dipole-dipole interactions dominate at holmium concentrations larger than 0.5%, and the observed linewidths exceed 1000 MHz in the sample containing about 1% of impurity Ho^{3+} ions.

IV. MODELING OF THE ELECTRON-PHONON INTERACTION AND SPIN-LATTICE RELAXATION RATES

We shall consider interactions of impurity Ho^{3+} ions with acoustical phonons with energies less than 40 K at liquid helium temperatures [energies of optical phonons in LiYF$_4$ are larger than 100 K (Ref. 25)]. The corresponding phonon wave lengths exceed essentially the lattice constants, and we can use the lattice elasticity theory to describe corresponding dynamic lattice deformations.

In the linear approximation, the Hamiltonian of the electron-phonon interaction corresponding to the modulation of the crystal field by elastic waves can be written as[26]

$$H_{e\text{-}ph} = \sum_{\Gamma j \lambda} \sum_{pk} B_{p,\lambda}^k(\Gamma^j) e_\lambda(\Gamma^j) a_p O_p^k$$

$$+ i \sum_\alpha \vartheta_\alpha [H_{CF} + H_{hf} + H_Z, (J_\alpha + I_\alpha)]. \quad (21)$$

Here the first and second terms on the right describe the electron-deformational and electron-rotational interactions, respectively. Linear combinations $e_\lambda(\Gamma^j)$ of the deformation tensor components ($e_{\alpha\beta}$) which transform according to irreducible representations of the factor group C_{4h} of the lattice [$e(A_g^1) = e_{zz}$, $e(A_g^2) = (e_{xx} + e_{yy})/2$, $e(B_g^1) = e_{xx} - e_{yy}$, $e(B_g^2) = e_{xy}$, $e_1(E_g) = e_{xz}$, $e_2(E_g) = e_{yz}$] and the rotation vector ϑ are linear in the phonon annihilation (a_{jq}) and creation (a_{jq}^+) operators. In particular,

$$e_{\alpha\beta} = \sum_{q, j = j_{ac}} \frac{q}{\sqrt{Nm}} [\alpha\beta, 1] \left(\frac{\hbar}{2\omega_j(\mathbf{q})} \right)^{1/2} (a_{j\mathbf{q}} + a_{j-\mathbf{q}}^\dagger), \quad (22)$$

where

$$[\alpha\beta, \sigma] = \frac{1}{2} (e_\alpha(j\mathbf{q}_0) q_{0\beta} + \sigma e_\beta(j\mathbf{q}_0) q_{0\alpha}), \quad \sigma = \pm 1,$$

$$(23)$$

the sum is taken over acoustical branches j_{ac} of the lattice vibrational spectrum, N is the number of unit cells having the mass m, and $e_\alpha(j_{ac}\mathbf{q}_0)$ are the components of the unit polarization vector in the elastic wave with the unit propagation vector $\mathbf{q}_0 = \mathbf{q}/q$ and the frequency $\omega_j(\mathbf{q})$. The components of the rotation vector θ_γ are given by the same expression (22) where $[\alpha\beta, -1]$ is substituted for $[\alpha\beta, 1]$ and $\alpha \neq \beta \neq \gamma$. Parameters of the electron-deformational interaction,

$$B_p^k(A_g^1) = B_{p,zz}^k,$$

$$B_p^k(A_g^2) = B_{p,xx}^k + B_{p,yy}^k,$$

$$B_p^k(B_g^1) = (B_{p,xx}^k - B_{p,yy}^k)/2,$$

$$B_p^k(B_g^2) = 2B_{p,xy}^k, \quad (24)$$

$$B_{p,1}^k(E_g) = 2B_{p,xz}^k,$$

$$B_{p,2}^k(E_g) = 2B_{p,yz}^k,$$

can be computed if the crystal field parameters for an impurity rare-earth ion are known as explicit functions of coordinates $X_{\lambda L, \alpha}$, of the host lattice ions (the vector $\mathbf{R}_{\lambda L}$ defines the equilibrium position of an ion λ in the unit cell L). The corresponding calculations were carried out in the framework of the exchange charge model of the crystal field.[26] Parameters of the crystal field Hamiltonian are represented by a sum of two terms,

$$B_p^k = e^2 K_p^k \sum_{\lambda L} \left[-Z_\lambda (1 - \sigma_p) \frac{\langle r^p \rangle}{R_{\lambda L}^{p+1}} + \frac{2(2p+1)}{7 R_{\lambda L}} S_p(R_{\lambda L}) \right] O_p^k(\vartheta_{\lambda L}, \varphi_{\lambda L}), \quad (25)$$

related to the electrostatic fields of point lattice ions with the effective charges eZ_λ and "exchange" charges at the neighbor ions proportional to the quadratic forms of the overlap integrals of the $4f$-electron and ligand wave functions $S_s = \langle 4f0 | n''s0 \rangle$, $S_\sigma = \langle 4f0 | n''p0 \rangle$, and $S_\pi = \langle 4f1 | n''p1 \rangle$ (only outer filled $n''s^2$ and $n''p^6$ electronic shells of ligand ions are considered):

$$S_p(R) = G_s S_s^2(R) + G_\sigma S_\sigma^2(R) + \left(2 - \frac{p(p+1)}{12} \right) G_\pi S_\pi^2(R). \quad (26)$$

Here K_p^k are the numerical coefficients,[26] σ_p are the shielding constants, $\langle r^p \rangle$ are the moments of the $4f$-electron charge density, and $O_p^k(\vartheta, \varphi)$ are the homogeneous Stevens polynomials formed from the direction cosines of ligand radius vectors (the spherical coordinates of a ligand are R, ϑ, φ relative to the rare-earth ion at the origin). Calculations were performed with $\sigma_2 = 0.579$, $\sigma_4 = \sigma_6 = 0$,[27] $\langle r^2 \rangle = 0.695$, $\langle r^4 \rangle = 1.219$, $\langle r^6 \rangle = 4.502$ (atomic units),[28] the lattice sums were computed by the Ewald method, and the dependences of the overlap integrals (computed with the radial wave functions from Refs. 29 and 30) on the distance R (in atomic units) between the ions were approximated by functions $S_0 \exp(-bR)$ where $S_0 = 2.2298$, 0.6535, and 1.3239 and $b = 1.2554$, 0.88259, and 1.1596 for s, σ, and π bonds, respectively. The values of the model parameters $G_s = G_\sigma = 5.6$ and $G_\pi = 2.85$ were obtained from fitting the calculated crystal field energies to the experimental data. The model results in the set of crystal field parameters (Table I, column 3) which are well comparable with those found from the analysis of the optical and EPR spectra (Table I, column 2).[9] The coupling constants $B_{p,\lambda}^k(\Gamma^j)$ in the Hamiltonian of the electron-deformational interaction presented in Table I (columns 4, 5, 8, 10, 12, 13, 15, and 16) were calculated using the same parameters of the model.

Now we have in hands all the data which are necessary to calculate the single-phonon transition probabilities introduced in Sec. II:
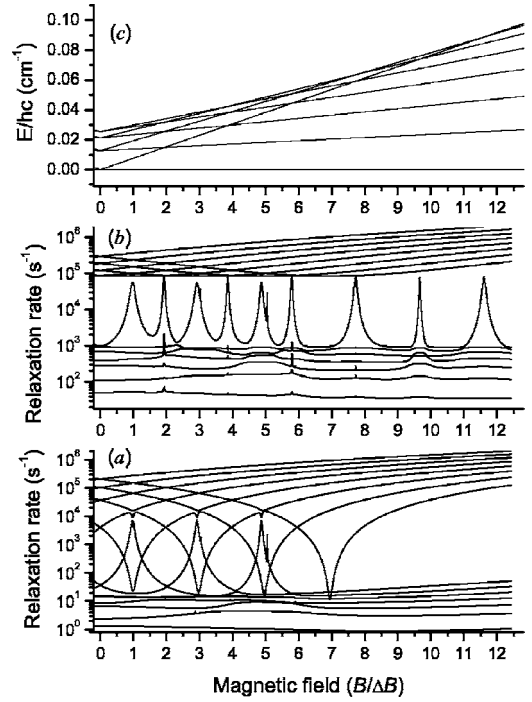

FIG. 4. Electron-phonon relaxation rates of a single Ho^{3+} ion in the phonon bath at the temperature 2 K. (a) Calculated eigenvalues of the relaxation matrix defined in the space of 16 electron-nuclear sublevels of the ground doublet, (b) calculated lower relaxation rates corresponding to one-phonon transitions between all sublevels of the ground doublet and the first singlet, and (c) relative energies of the electron-nuclear sublevels of the first excited singlet in the magnetic field $\mathbf{B} \| c$.

$$W_{m \to f} = \frac{\omega_{mf}^3}{\pi \hbar \rho} \sum_{j=j_{ac}} \int \frac{\sin \theta d\theta d\varphi}{4\pi v_j^5(\theta\varphi)} \left| \sum_{\alpha\beta} \left\langle f \left| \sum_{pk} B_{p,\alpha\beta}^k [\alpha\beta, +1] \right. \right. \right.$$
$$\left. \left. \left. \times a_p O_p^k + i\hbar \omega_{fm} [\alpha\beta, -1] \sum_\gamma \varepsilon_{\alpha\beta\gamma} (J_\gamma + I_\gamma) \right| m \right\rangle \right|^2$$
$$\times [n_0(\omega_{mf}) + 1]. \quad (27)$$

Here $\varepsilon_{\alpha\beta\gamma}$ is the unit antisymmetric tensor and $v_j(\theta\varphi)$ is the sound velocity in the direction of the phonon wave vector $\mathbf{q}$ determined by the angular coordinates θ and φ. The integrals $\Sigma_{j=j_\alpha} \int [\alpha\beta, \sigma][\gamma\delta, \sigma'] d\Omega / 4\pi v_{j\alpha}^5$ were computed in Ref. 31.

The analysis of the magnetic field and temperature dependences of the relaxation rates involved the numerical diagonalization of the matrix of the Hamiltonian H_0 [see Eq. (19)] for the fixed values of the magnetic field (the matrix was constructed in the space of 136 functions $|{}^5I_8, JJ_z \rangle \otimes |II_z \rangle$ of the lowest multiplet), calculations of transition probabilities for each pair of the electron-nuclear sublevels using the corresponding eigenfunctions of H_0, and the diagonalization of the relaxation matrix $\mathbf{W}$. Figure 4(a) shows the magnetic field dependences at the temperature 2 K of the eigenvalues of the relaxation matrix defined in the subspace of sublevels of the ground doublet. In this case transitions are mainly induced by the dynamic deformations of B_g symmetry between the sublevels with the same projections of the nuclear spin. However, mixing of wave functions of the ground dou-

TABLE II. Splittings of non-Kramers doublets in LiYF$_4$:Ho^{3+} (1%) crystals axially compressed in the basis plane. Results of calculations are in brackets.

N	Energy of Γ_{34} (cm^{-1})		Splitting $\Delta(\varphi)$ (cm^{-1}/100 MPa)		
			$\varphi=5°$	$\varphi=30.7°$	$\varphi=45°$
1	$^5I_8$	0	0.33 (0.43)	0.67 (0.63)	0.53 (0.53)
2	$^5I_8$	72	1.12 (1.50)	1.50 (1.98)	1.14 (1.57)
3	$^5I_6$	8686	0.62 (0.37)	0.71 (0.35)	0.38 (0.21)
4	$^5I_6$	8783	1.90 (1.43)	2.20 (1.93)	2.00 (1.56)
5	$^5I_5$	11240	0.34 (0.49)	0.44 (0.45)	0.34 (0.30)
6	$^5I_5$	11248	0.43 (0.53)	0.50 (0.78)	0.53 (0.68)
7	$^5I_5$	11327	1.45 (1.33)	1.95 (1.77)	1.60 (1.42)
8	$^5F_5$	15491	0.52 (0.72)	0.67 (0.90)	0.62 (0.85)
9	$^5F_5$	15620	1.01 (1.02)	1.18 (1.33)	0.82 (1.05)

blet with the wave functions of the excited singlets allows transitions with the nuclear spin reverting as well. At high magnetic fields ($B > 0.18$ T), there are two sets of solutions, each consisting of eight branches corresponding to allowed (fast relaxation rates exceeding 10^3 s^{-1}) and forbidden (slow relaxation rates less than 10^2 s^{-1}) transitions (of course, there is always a zero solution corresponding to the equilibrium state of the system). At lower magnetic fields we see specific variations of four upper branches at the $\Delta m = 0$ anticrossings and of three lower branches at the $\Delta m = 2$ anticrossings pointed out in Fig. 2. The additional narrow peaks superimposed on the broad peaks are caused by more narrow $\Delta m = -2$ anticrossings which are shifted from the $\Delta m = 2$ anticrossings along the magnetic field axis because the spectrum is only approximately equidistant.

Figure 4(b) demonstrates a remarkably different behavior of the considered single-ion relaxation rates at the same temperature, 2 K, when the transitions between the first excited singlet and the ground doublet are taken into account (these transitions are induced by lattice deformations of E_g symmetry). There are again two sets of fast and slow relaxation rates, but all rates become larger by one to two orders of magnitude, the dips at the $\Delta m = 0$ anticrossings disappear, and six additional peaks in the lower branches are observed due to the anticrossings between the sublevels of the first excited singlet Γ_2 which are shown in Fig. 4(c). It follows from the results of calculations of the relaxation rates at liquid helium temperatures that the frequency dependence of the out-of-phase susceptibility of Ho^{3+} ions should exhibit a maximum at frequencies close to 10^5–10^6 Hz contrary to the earlier observations[2] of this maximum at frequencies below 10^3 Hz. This contradiction stimulated us to test the theory by direct measurements of the electron-phonon coupling constants in the piezospectroscopic experiments described in the following section.

V. EXPERIMENT

A. Piezospectroscopic measurements

To determine parameters of the Hamiltonian (21) corresponding to the interaction of the Ho^{3+} ion with lattice strains

of B_g symmetry, we measured splittings of nine Γ_{34} doublets (see Fig. 1) induced by the uniaxial stress applied in the basis plane of the lattice. The sample LiYF$_4$ containing 1 at % of holmium was grown by the Bridgman-Stockebarger method and oriented with the x-ray diffractometer. Experiments were performed at temperatures 4.2 K and 77 K; pressure p up to 220 MPa was supplied along three different directions in the (001) plane. Splittings of the optical lines corresponding to singlet-doublet transitions in the σ-polarized absorption spectra (the wave vector of the incident light was parallel to the c axis) were measured directly or from the linear dichroism signals.[20]

The uniaxial pressure in the plane (001) at the angle φ relative to the a axis induces the following nonzero components of the deformation tensor:

$$e(A_g^1) = -S_{13}p,$$

$$e(A_g^2) = -(S_{11} + S_{12})p/2,$$

$$e(B_g^1) = -[(S_{11} - S_{12})\cos 2\varphi + S_{16} \sin 2\varphi]p,$$

$$e(B_g^2) = -(2S_{16}\cos 2\varphi + S_{66}\sin 2\varphi)p/4.$$

Here S_{ij} are the components of the elastic compliance tensor of LiYF$_4$ measured in Ref. 32, in particular $S_{11} - S_{12} = 18.6$, $S_{16} = 8.01$, and $S_{66} = 57.7$ (10^{-6}/MPa). In the linear approximation, the corresponding splitting of the doublet with the wave functions $|\Gamma_{34}\pm\rangle$ equals

$$\Delta(\Gamma_{34}, \varphi) = 2\left|\left\langle \Gamma_{34} + \left| \sum_{pk, i=1,2} B_p^k(B_g^i)e(B_g^i)a_p O_p^k \right| \Gamma_{34} - \right\rangle\right|$$

$$= p[C + D\cos(4\varphi - \varphi_0)]^{1/2}. \quad (28)$$

Using the data obtained at three different values of the angle φ (see Table II), we determined for each doublet the corresponding deformation potentials C and D and the directions φ_0 of the petals of the fourfold rosettes (28). Then the set of 16 electron-deformation parameters $B_p^k(B_g^i)$ ($p k \rightarrow 2\,2,\ 2-2,\ 4\,2,\ 4-2,\ 6\,2,\ 6-2,\ 6\,6,\ 6-6$) was varied starting from the values obtained in the framework of the exchange charge model (Table I, columns 8 and 10) to obtain
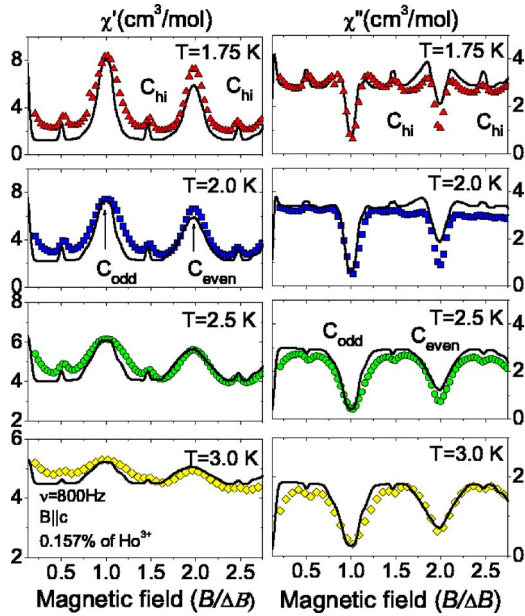
FIG. 5. (Color online) Measured (symbols) and simulated (solid curves) magnetic field dependences of the ac susceptibility in LiYF$_4$:Ho^{3+} (0.157%) at different temperatures ($\nu=800$ Hz, **B**$\|c$).
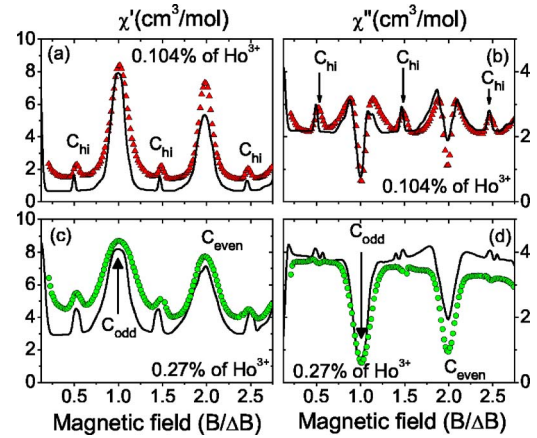

FIG. 6. (Color online) Measured (symbols) and simulated (solid curves) magnetic field dependences of the ac susceptibility at the temperature 1.75 K in LiYF$_4$:Ho^{3+} samples with different holmium concentrations x [(a), (b) $x=0.104\%$, (c), (d) $x=0.27\%$, $\nu=800$ Hz, **B**$\|c$].

the best estimations of the measured splittings. Results of the fitting procedure are given in Table I (columns 7 and 9), and the calculated and experimental splittings are compared in Table II. We had only 18 independent nonlinear equations for 16 variables. It should be noted that the positive direction of the b axis relative to the a axis was unknown, and signs of angles φ were checked in the fitting procedure. Possible errors in the measured splittings (in particular, due to random internal strains and errors in the orientation of the sample) are rather large (±0.15 cm^{-1}/100 MPa), the linear approximation for some closely spaced doublets (having numbers 3, 5, and 6 in Table II) is not valid, and the parameters $B_p^k(B_g^i)$ have not been determined unambiguously. However, as is seen in Table I the final set of parameters $B_p^k(B_g^i)$ does not differ qualitatively from the starting values. Thus, the model used in calculations of the parameters of the electron-phonon interaction has been additionally approved. A possible error in the estimations of the matrix elements of electronic operators in the Hamiltonian of electron-phonon interaction (21) which we need to calculate the transition probabilities between the sublevels of the ground doublet does not exceed 24%.

B. Measurements of the dynamic susceptibility

Earlier the dynamic susceptibility of diluted LiY$_{1-c}$Ho$_c$F$_4$ crystals with holmium concentrations $c=46\%$, 16.7%, and 4.5% was studied in Refs. 33–35 at low temperatures with main attention for the spin-glass behavior in a random dipolar-coupled Ising magnet.

In the present work, the dynamic susceptibility of highly diluted LiY$_{1-c}$Ho$_c$F$_4$ single crystals was measured with a conventional superconducting quantum interference device (SQUID) magnetometer at frequencies from 20 to 1200 Hz

in the temperature range 1.75–4 K. Three samples with dimensions of $4\times4\times10$ mm^3 were studied in collinear ac and dc magnetic fields parallel to the c axis of amplitude of 4 10^{-4} T and up to 0.25 T, respectively. The holmium concentrations in these samples ($c=0.104\%$, 0.157%, 0.27%) were determined by a comparison of the measured low-frequency susceptibility with the calculated single-ion static susceptibility. The in- and out-of-phase susceptibility was measured in a more extended dc field, frequencies, temperatures, and concentrations, than in Ref. 2, where the results of measurements of the in- and out-of-phase susceptibilities at frequencies 163 and 800 Hz in the sample with holmium concentration $c=0.04\%$ were published.

The results presented in Figs. 5–7 show the nonmonotonous behavior with well-pronounced peaks and dips at dif-
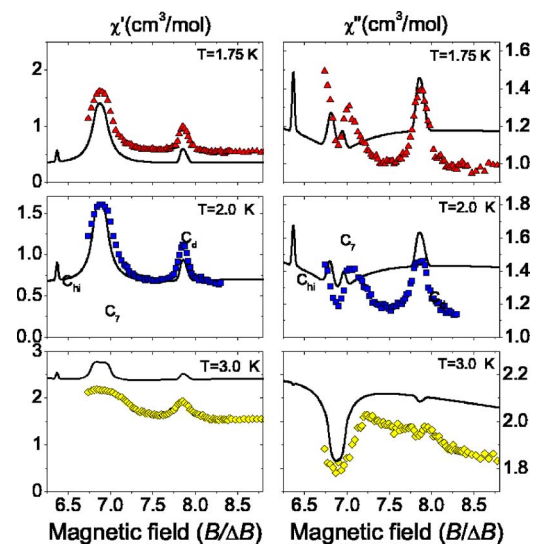

FIG. 7. (Color online) Measured (symbols) and simulated (solid curves) magnetic field dependences of the ac susceptibility in LiYF$_4$:Ho^{3+} (0.104%) in the region of high-field crossings at different temperatures ($\nu=1200$ Hz, **B**$\|c$).
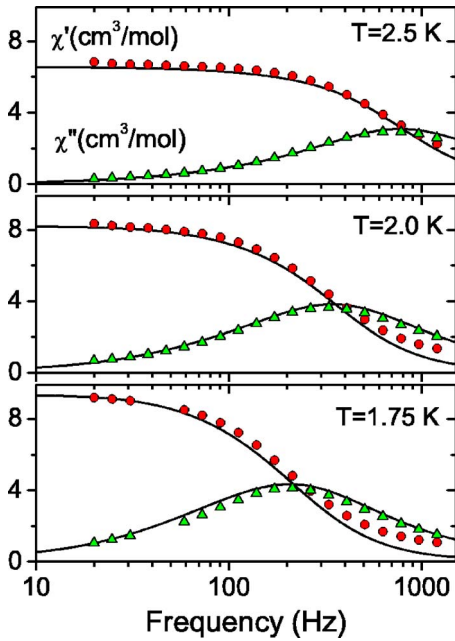
FIG. 8. (Color online) Measured (symbols) and simulated (solid curves) frequency dependences of the dynamic susceptibility in LiYF$_4$:Ho^{3+} (0.104%) at different temperatures (**B**$\|c$, B =38.5 mT).

FIG. 10. (Color online) Measured (symbols) and simulated (solid curves) temperature dependences of the dynamic susceptibility in LiYF$_4$:Ho^{3+} (0.104%) at different frequencies of the ac magnetic field (**B**$\|c$, B=38.5 mT).

ferent crossing points of the electron-nuclear energy levels. In particular, the out-of-phase susceptibility measured in the vicinity of the crossing points for two holmium concentrations shows an inversion of the sign of C_{hi} peaks (dips) with respect to the background (Fig. 6). Figure 8 presents the frequency dependences of the in- and out-of-phase susceptibilities at three different temperatures while the temperature and concentration shifts of the out-of-phase susceptibility with frequency are given in Fig. 9. Note that in both cases the dc magnetic field was taken in between two single-ion electron-nuclear crossing points (38.5 mT, corresponding to
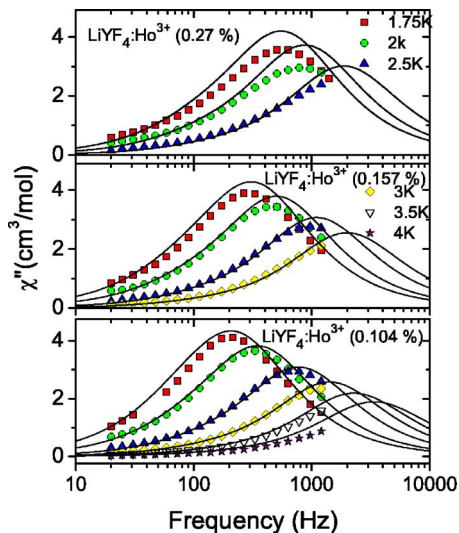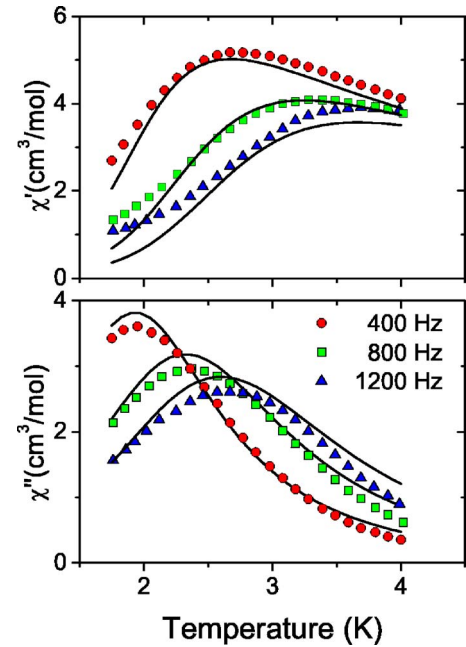
1.62ΔB). The temperature dependences of the in- and out-of-phase susceptibilities at different ac frequencies are shown in Fig. 10.

VI. SIMULATIONS OF THE DYNAMIC SUSCEPTIBILITY IN LiYF$_4$:Ho^{3+} AND DISCUSSION

The experimental data presented in Figs. 5–10 are accompanied by results of the corresponding simulations. Calculations of the susceptibilities involved the numerical diagonalization of the single ion Hamiltonian H_0 [see Eq. (19)] in the space of 136 electron-nuclear states of the lowest $^5I_8$ multiplet for the fixed values of the external magnetic field, the computing of the matrix elements of electronic operators which are necessary to construct the relaxation matrices (14) and (27), and at the last step $\chi'(\omega) = \mathrm{Re}\chi_{zz}(\omega)$ and $\chi''(\omega) = \mathrm{Im}\chi_{zz}(\omega)$ were obtained at different frequencies and temperatures using the expression (8).

First of all, let us consider the frequency dependences of the out-of-phase susceptibilities in Fig. 9 measured at the dc magnetic field value of 1.62ΔB, which is far enough from the neighboring single-ion crossing points. The maximum of the out-of-phase susceptibility shifts to higher frequencies with the increasing temperature. These shifts give evidence for the increasing relaxation rates induced by the electron-phonon interaction. However, using the one-phonon transition probabilities calculated with the parameters of the electron-deformational interaction from Table I, we found the corresponding maxima at the frequencies 10^4–10^5 Hz (see Fig. 4 with the plotted relaxation times), which are about two orders of magnitude higher than the experimental values. Even more, Fig. 9 also shows a concentration dependence of the
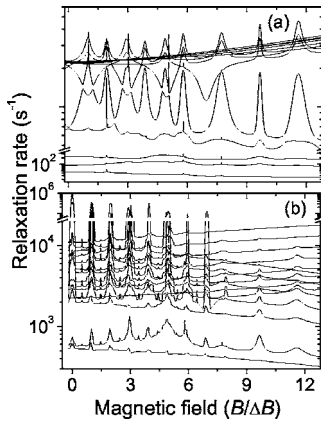

FIG. 9. (Color online) Measured (symbols) and simulated (solid curves) frequency dependences of the out-of-phase susceptibility in LiYF$_4$:Ho^{3+} samples at different temperatures (**B**$\|c$, B=38.5 mT).

FIG. 11. The phonon bottleneck and cross-relaxation effects on the relaxation rates. (a) The relaxation rates at the temperature 2 K in the sample $LiYF_4$:Ho^{3+} (0.104%) calculated with the renormalized electron-phonon transition probabilities due to the bottleneck effect (b) and results of calculations with the cross-relaxation terms taken into account.

FIG. 12. The simulated ac susceptibility of the $LiYF_4$:Ho^{3+} (0.27%) sample at the frequency 800 Hz and temperature 2 K; the magnetic field is declined from the c axis by $1°$. (a) The relaxation matrix contains only one-phonon transition probabilities calculated with the electron-phonon coupling constants presented in Table I (b) the transition probabilities are renormalized due to the phonon bottleneck effect, and (c) the cross-relaxation terms are included.

maximum of the out-of-phase susceptibility, while it is clear that single-ion electron-phonon interaction cannot produce any dependence of the relaxation rate on the concentration of relaxing ions. Thus, to fit the simulated frequency dependences to the experimental curves, we had to take into account the phonon bottleneck effect. The concentration dependence of the renormalized transition probability (18) is determined by a factor $K_{mk} = \tau_{ph}(\omega_{mk})N/\Delta\omega_{mk}$. Using the average sound velocity $v = 3 \times 10^3$ m/s,[32] the number of paramagnetic ions per unit volume, $N = 2c/V$ [here V is the unit cell volume which contains two Y^{3+} sites accessible for holmium ions, and c is the concentration determined from measurements of $\chi'(\omega \to 0)$], and the widths of spectral distributions of the resonant phonons $\Delta\omega_{mk} = 2\gamma_{mk} = 300$ MHz according to the EPR data on the widths of the singlet-doublet transitions,[9] we found it necessary to introduce two different phonon lifetimes independent of temperature to describe the experimental data for the sample with the concentration $c = 0.104\%$ (see Figs. 8 and 9). Namely, we used $\tau_{ph}(\omega) = \tau_g \sim 1$ μs for resonant phonons with frequencies corresponding to transitions between the electron-nuclear sublevels of the ground electronic doublet and $\tau_{ph}(\omega) = \tau_s \sim 0.1$ μs for phonons with frequencies corresponding to transitions between the excited singlet and the ground doublet. Actually, the transitions between the electron-nuclear sublevels of the ground doublet are narrower than the transitions between the sublevels of the singlet and doublet crystal field states, and the lifetimes τ_g and τ_s may differ less than by order of magnitude. However, to fit the measured frequency dependences of the susceptibilities in the samples with higher concentrations of holmium ions, we had to diminish the factors K_{mk} by 1.48 ($c = 0.157\%$) and 2.7 ($c = 0.27\%$) times as compared with these factors for $c = 0.104\%$. Thus, despite the increase of the concentration of the paramagnetic ions, the phonon bottleneck effect weakens due to broadening of the spectral bands of the resonant phonons and possible decrease of the phonon lifetimes.

To illustrate the phonon bottleneck effect on the relaxation rates, we present in Fig. 11(a) the calculated rates in the
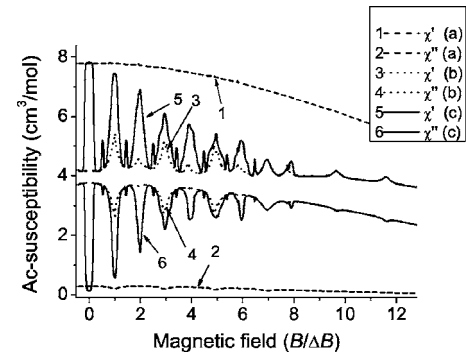
sample with the concentration $c = 0.104\%$ versus the magnetic field. These rates are condensed within the much narrower range as compared with the relaxation rates represented in Figs. 4(a) and 4(b); the damping effect of the gaps at the $\Delta m = 0$ crossings is partly restored due to the strong suppression of the singlet-doublet transition probabilities, but there are still no remarkable variations of the lower branches at the crossing points which may be expected in accordance with the measured field dependences of the in- and out-of-phase susceptibilities represented in Figs. 5–7.

As is seen in Fig. 12 the magnetic field dependences of χ' and χ'' obtained without phonon bottleneck and cross-relaxation effects (with electron-phonon transition probabilities only, curves 1 and 2) have nothing in common with the experimental data (Figs. 5–7). When making use of electron-phonon transition probabilities renormalized by phonon bottleneck, we obtain the curves 3 and 4 showing some overlap with the measured ones (the specific humps and dips appear at the odd crossing points) but their "intensities" are lower than the experimental ones, and also there is no sign of corresponding features at even and half-integer crossings. However, the results dramatically change when the cross relaxation is taken into account: in this case all crossing points manifest themselves properly (the curves 5 and 6) and are very close to the experimental results.

The cross-relaxation rates were calculated assuming the Gaussian line shape $g^{CR} = (2\pi\Delta)^{-1} \exp[-(\omega_{pn} - \omega_{lm})^2/2\Delta^2]$ of the spectral density of the energy reservoir corresponding to interactions between the holmium ions. It is enough to consider in Eq. (14) only three nonzero fitting parameters k_{12} and k_{66}, which determine the transition probabilities within the manifold of the electron-nuclear sublevels of the ground doublet, and k_{44}, which determines rates of the singlet-doublet transitions. For the scaling factor $\delta = 2 \times 10^8$ s^{-1}, the fixed values of $k_{12} = k_{66} = 0.1$ and $k_{44} = 0.004$ independent of the concentration of the holmium ions were used in all calculations. However, the dispersion Δ of frequencies of the cross-relaxation transitions depends on the concentration; it was estimated from the EPR linewidths and corrected from a

comparison of the simulated field dependences with the experimental data ($\Delta=100$, 120, and 140 MHz for the g_{44}^{CR} line shape and $\Delta=185$, 200, and 240 MHz for the g_{12}^{CR} and g_{66}^{CR} line shapes for samples with concentrations 0.104, 0.157, and 0.27%, respectively). As it is seen in Fig. 11(b), the cross-relaxation rates play the dominant role at all crossing points. The most important result of the cross-relaxation processes is the appearance of the low-frequency (10^2–10^3 s^{-1}) branch in the spectrum of relaxation rates with the well-resolved maxima at the crossing points. It should be noted that the calculated field dependences of the relaxation rates may change remarkably when using another cross-relaxation line shapes (the Lorentz distributions, in particular),[11] but to analyze this problem it is necessary to perform measurements in the samples with a more wide range of concentrations of paramagnetic ions.

Small peaks at the half-integer crossings in the field dependences of χ' (and the peaks and dips at these points in the field dependences of χ'') are induced by the cross-relaxation singlet-doublet transitions (they disappear in the simulated curves for $k_{44}=0$). The value of the parameter k_{44} used in simulations (the results are represented in Figs. 5–7) coincides by an order of magnitude with the estimation based on the assumption of the prevailing role of the magnetic dipole-dipole interactions:

$$k_{44} = 2\pi c a^6 \sum \left(\frac{3xz}{r^5}\right)^2.$$

Here the sum is taken over all Y^{3+} sites, a is the lattice constant, and c is the concentration of impurity holmium ions. However, values of the parameters k_{12} and k_{66} mentioned above are much larger than the similar estimations, and it is possible that the virtual phonon exchange contributes essentially into the interaction between the holmium ions in the ground state, in particular due to strong coupling with the dynamic lattice deformations of B_g symmetry.

The peaks C_d in the high-field dependences of χ' and χ'' close to the magnetic field value $B=8\Delta B$ in Fig. 7 correspond to the anticrossing of the electron-nuclear sublevels of the excited singlet (see Fig. 4). These peaks appear due to a combined action of the random crystal field [described by the Hamiltonian H_S; see Eq. (19)] and the cross-relaxation processes (singlet-doublet transitions). So we had a possibility to determine independently the k_{44} parameter from fitting intensities of C_{hi} peaks and parameters of the Hamiltonian H_S from fitting intensities of the C_d peaks. The best fit was achieved when the parameters B_2^2 and B_2^{-2} from Ref. 9 (see Sec. III above) were increased by a common factor of 1.5, 1.8, and 3.3 for samples studied in this work with holmium concentrations 0.104%, 0.157%, and 0.27%, respectively, and natural abundances of Li isotopes. It should be noted that we have not succeeded in exact description of measured real and imaginary parts of the dynamic susceptibilities at any frequency, temperature, and external magnetic field values. In particular, we obtained correct positions of the maxima in the frequency dependences of the out-of phase susceptibilities, but the calculated maximum values are higher than the measured data (see Fig. 9). The discrepancies between theory

and experiment in Fig. 7 are the consequences of this lack of the theory. However, the specific behavior of the susceptibility in the vicinity of high-field anticrossings is reproduced by calculations as well. To derive a more elaborated model, we need additional experimental data at higher frequencies.

It follows from the simulations that an additional narrow peak should split out from the peak C_d in the plot of χ' versus the magnetic field (see curve 5 in Fig. 12) in the transverse magnetic field, in particular due to a rather small misalignment of the sample. Because such a peak was not observed, we had good reasons to believe that the samples were oriented with the accuracy better than 1°.

Using the model parameters determined from the analysis of the frequency and field dependences of χ' and χ'', we obtained a satisfactory description of the temperature dependences as well (see Fig. 10). The transformations of the magnetic field dependences of the out-of-phase susceptibility at the fixed frequency in the vicinity of the crossing points with temperature (Figs. 5 and 7) or concentration (Fig. 6) can be explained as a result of strong variation of relaxation rates with the magnetic field at these points. If the effective relaxation rate exceeds the frequency of the ac field, χ'' has a dip, and if the relaxation rate is less than the frequency, χ'' has a peak at the crossing point. The corresponding "peak-to-dip" transformations can be easily recognized in Figs. 5–7.

VII. CONCLUSION

We conclude that the microscopic model of a linear non-resonant response of the electron-nuclear subsystem in the highly diluted paramagnetic crystal $LiYF_4{:}Ho^{3+}$ on the weak ac field has been derived. The model operates with a few phenomenological parameters introduced to account for a finite heat capacity of the resonant phonons and cross-relaxation processes. The finite phonon lifetimes independent of temperature of about 1 μs, comparable with the phonon time of flight between the sample boundaries, have been determined from fitting the results of calculations to the measured frequency dependences of out-of-phase susceptibilities in the samples with different holmium concentrations. The parameters of the interaction between paramagnetic ions, which determine cross-relaxation rates, were obtained from fitting the simulated dependences of in-phase and out-of-phase susceptibilities on the external magnetic field. The obtained value of the parameter k_{44}, which defines co-tunneling processes at half-integer crossing points in the spectrum of a pair of Ho^{3+} ions, agrees with the estimation based on the dipole-dipole mechanism of interion coupling. However, to present definite conclusions about the most important terms in the Hamiltonian of interaction between the holmium ions, which are responsible for the cross-relaxation processes at integer crossing and anti crossing points, it is necessary to derive a more elaborated theory of cross relaxation than the high-temperature approach of Ref. 5.

The model containing a single-ion crystal field including random strains, electron-phonon transitions including bottleneck, hyperfine, and cross-spin interactions is comprehensive and can be used to predict the detailed magnetization dynamics in $LiYF_4{:}Ho^{3+}$ crystals at ultralow temperatures and at

higher frequencies. Note that half-integer transitions were observed at elevated temperatures (above 1.5 K) only in ac susceptibility experiments or at fast sweeping field in the low-temperature (below 0.1 K) magnetization measurements where the bottleneck effects stabilized an effective spin-phonon temperature of half a kelvin.[2,3,6] In the present theoretical approach half-integer transitions result from resonant cross-relaxation transitions involving sublevels of the lower singlet with the activation energy of $\sim$10 K, which is satisfactory to fit the experimental data taken at liquid helium temperatures. A more detailed analysis of the magnetization dynamics in the sweeping fields will be presented in a separate paper. The theory may be additionally tested by measurements of the ac susceptibility and NMR in a tilted magnetic field. Finally, this theoretical approach may be also expanded to other magnetic systems, in particular the single-molecule magnets.

[1] K. H. Hellwege, J. Kotzler, and G. Weber, Z. Phys. **217**, 373 (1968).

[2] R. Giraud, A. M. Tkachuk, and B. Barbara, Phys. Rev. Lett. **91**, 257204 (2003).

[3] R. Giraud, W. Wernsdorfer, A. M. Tkachuk, D. Mailly, and B. Barbara, Phys. Rev. Lett. **87**, 057203 (2001).

[4] L. Thomas, F. Lionti, R. Ballou, D. Gatteschi, R. Sessoli, and B. Barbara, Nature (London) **383**, 145 (1996).

[5] N. Bloembergen, S. Shapiro, P. S. Pershan, and J. O. Artman, Phys. Rev. **114**, 445 (1959).

[6] B. Barbara, R. Giraud, W. Wernsdorfer, D. Mailly, P. Lejay, A. Tkachuk, and H. Suzuki, J. Magn. Magn. Mater. **272-276**, 1024 (2004).

[7] E. S. Grinberg, A. V. Duglav, and B. I. Kochelaev, Zh. Eksp. Teor. Fiz. **82**, 888 (1982).

[8] M. J. Graf, A. Lascialfari, F. Borsa, A. M. Tkachuk, and B. Barbara, Phys. Rev. B **73**, 024403 (2006).

[9] G. S. Shakurov, M. V. Vanyunin, B. Z. Malkin, B. Barbara, R. Yu. Abdulsabirov, and S. L. Korableva, Appl. Magn. Reson. **28**, 251 (2005).

[10] M. N. Leuenberger and D. Loss, Phys. Rev. B **61**, 1286 (2000).

[11] T. Pohjola and H. Schoeller, Phys. Rev. B **62**, 15026 (2000).

[12] P. Santini, S. Carretta, E. Liviotti, G. Amoretti, P. Carretta, M. Filibian, A. Lascialfari, and E. Micotti, Phys. Rev. Lett. **94**, 077203 (2005).

[13] S. A. Al'tshuler and B. M. Kozirev, *Electron Paramagnetic Resonance* (Nauka, Moscow, 1972).

[14] J. M. Baker, J. Phys. C **4**, 1631 (1971).

[15] J. H. Van-Vleck, Phys. Rev. **59**, 724 (1941); **59**, 730 (1941).

[16] E. Garcia and R. R. Ryan, Acta Crystallogr., Sect. C: Cryst. Struct. Commun. **49**, 2053 (1993).

[17] N. Karayianis and D. E. Wortman, J. Phys. Chem. Solids **37**, 675 (1976).

[18] N. I. Agladze and M. N. Popova, Solid State Commun. **55**, 1097 (1985).

[19] B. M. Walsh, G. W. Grew, and N. P. Barnes, J. Phys.: Condens. Matter **17**, 7643 (2005).

[20] A. V. Vinokurov, B. Z. Malkin, A. I. Pominov, and A. L. Stolov, Fiz. Tverd. Tela (Leningrad) **28**, 381 (1986) [Sov. Phys. Solid State **28**, 211 (1986)].

[21] R. Yu. Abdulsabirov, A. A. Kazantsev, S. L. Korableva, B. Z. Malkin, S. I. Nikitin, and A. L. Stolov, J. Lumin. **117**, 225 (2006).

[22] S. A. Al'tshuler, V. I. Krotov, and B. Z. Malkin, Pis'ma Zh. Eksp. Teor. Fiz. **32**, 232 (1980) [JETP Lett. **32**, 214 (1980)].

[23] L. A. Bumagina, V. I. Krotov, B. Z. Malkin, and A. Kh. Khasanov, Zh. Eksp. Teor. Fiz. **80**, 1543 (1981) [Sov. Phys. JETP **53**, 792 (1981)].

[24] J. P. D. Martin, T. Boonyarith, and N. B. Manson, J. Lumin. **63**, 297 (1995).

[25] S. Salaun, A. Bulou, M. Rousseau, B. Hennion, and J. Y. Gesland, J. Phys.: Condens. Matter **9**, 6957 (1997).

[26] B. Z. Malkin, in *Spectroscopy of Solids Containing Rare-earth Ions*, edited by A. A. Kaplyanskii and R. M. Macfarlane (Elsevier, Amsterdam, 1987), Chap. 2, pp. 13–49.

[27] P. Erdos and J. H. Kang, Phys. Rev. B **6**, 3393 (1972).

[28] A. J. Freeman and R. E. Watson, Phys. Rev. **127**, 2058 (1962).

[29] O. J. Sovers, J. Phys. Chem. Solids **28**, 1073 (1967).

[30] E. Clementi and A. D. McLean, Phys. Rev. **133**, A419 (1964).

[31] A. A. Antipin, L. A. Bumagina, B. Z. Malkin, and R. M. Rakhmatullin, Fiz. Tverd. Tela (Leningrad) **23**, 2700 (1981) [Sov. Phys. Solid State **23**, 1583 (1981)].

[32] P. Blanchfield and G. A. Saunders, J. Phys. C **12**, 4673 (1979).

[33] D. H. Reich, T. F. Rosenbaum, G. Aeppli, and H. J. Guggenheim, Phys. Rev. B **34**, 4956 (1986).

[34] D. H. Reich, T. F. Rosenbaum, and G. Aeppli, Phys. Rev. Lett. **59**, 1969 (1987).

[35] D. H. Reich, B. Ellman, J. Yang, T. F. Rosenbaum, G. Aeppli, and D. P. Belanger, Phys. Rev. B **42**, 4631 (1990).